MICRO-MACRO TRANSITION FOR AN-ISOTROPIC GRANULAR PACKINGS

Stefan Luding

Particle Technology, DelftChemTech, TU Delft,
Julianalaan 136, 2628 BL Delft, The Netherlands

e-mail: s.luding@tnw.tudelft.nl

Abstract
From the structure of a static granular solid, we derive the fabric-, the stress-, and the stiffness-tensor in average over pairs of interacting particles. Starting from a linear expansion of the interaction potential around static equilibrium, stress and strain can be derived from the principles of virtual displacement and virtual stress-change, respectively. Our approach includes both normal and tangential forces, and the influence of both is discussed separately. Finally, the results are applied to a discrete particle simulation where the averaged micro-quantities on the contact-level can be compared to the macroscopic observations on the boundaries of the system. An-isotropy in the bi-axial system is obtained and is directed against the direction of compression up to a certain (maximal) magnitude. In the critical state shear regime, the an-isotropy is considerably smaller.

1 Introduction

One of todays great challenges in material science and physics is the macroscopic description of the material behavior of granular media which are inhomogeneous, nonlinear, disordered, and anisotropic on a "microscopic" scale [1–3]. This is due to the stress distribution in granular assemblies and the corresponding stress-networks involving large fluctuations of contact forces and a reorganization of the network due to deformation. If an initially isotropic contact network is deformed, the result can be anisotropic in structure.

In this study, the anisotropic material tensor is computed from a discrete particle simulation of a biaxial box simulation, in average over many particles.

2 Micro-macro transition for one contact

The vector connecting the centers of mass $\boldsymbol{r}_1$ and $\boldsymbol{r}_2$ of two particles, is the so-called branch vector $\boldsymbol{l} = \boldsymbol{r}_1 - \boldsymbol{r}_2$, with the equilibrium distance $l = |\boldsymbol{l}| = 2a$ and the corresponding unit vector $\hat{\boldsymbol{n}} = \boldsymbol{l}/l$. The overlap in normal direction $\boldsymbol{\Delta} = \boldsymbol{l} - 2a\hat{\boldsymbol{n}} =: \boldsymbol{\epsilon}^n \cdot \boldsymbol{l}$,is defined relative to the configuration when the particles just touch each other. This defines $\boldsymbol{\epsilon}^n = \hat{\boldsymbol{n}}(\hat{\boldsymbol{n}} \cdot \boldsymbol{\epsilon})$, the

normal contribution of the deformation $\boldsymbol{\epsilon} = \boldsymbol{\epsilon}^n + \boldsymbol{\epsilon}^t$, relative to a virtual, stress-free reference configuration. The displacement in tangential direction $\boldsymbol{\vartheta} =: \boldsymbol{\epsilon}^t \cdot \boldsymbol{l}$,is irrelevant for perfectly smooth particles, but has to be taken into account for rough surfaces. This defines $\boldsymbol{\epsilon}^t = \hat{\boldsymbol{t}}(\hat{\boldsymbol{t}} \cdot \boldsymbol{\epsilon})$, the tangential contribution to $\boldsymbol{\epsilon}$. A virtual (small) change of the deformation is

$$\delta \boldsymbol{l} = \boldsymbol{l}' - \boldsymbol{l} =: \boldsymbol{\varepsilon} \cdot \boldsymbol{l} \approx \delta\Delta\hat{\boldsymbol{n}} + \delta\vartheta\hat{\boldsymbol{t}} \tag{1}$$

where the prime denotes the value after the deformation tensor $\boldsymbol{\varepsilon} := \delta\boldsymbol{\epsilon}$ is applied.

2.1 Change of the branch vector

When the packing of particles is deformed, it is most intuitive that the branch vector changes. This change, $\delta\boldsymbol{l}$, can be split in two components, one parallel to $\hat{\boldsymbol{n}}$, the other one perpendicular to it. The components of the normal change of $\boldsymbol{l}$ are $\delta\boldsymbol{\Delta} := \delta\boldsymbol{l}^n = \hat{\boldsymbol{n}}(\hat{\boldsymbol{n}} \cdot \boldsymbol{\varepsilon} \cdot \boldsymbol{l})$ and, expressed in index notation [1], read

$$\delta\Delta_\alpha = \delta l^n_\alpha = n_\alpha n_\beta \varepsilon_{\beta\gamma} l_\gamma \ . \tag{2}$$

The tangential components are $\delta\boldsymbol{\vartheta} := \delta\boldsymbol{l} - \delta\boldsymbol{l}^n$, or

$$\delta\vartheta_\alpha = \delta l^t_\alpha \ = \ t_\alpha t_\beta \varepsilon_{\beta\gamma} l_\gamma \ , \tag{3}$$

with the intrinsic definition of the tensor $t_\alpha t_\beta$ perpendicular to $n_\alpha n_\beta$. The unit-tensor is replaced by the Kronecker-delta $1_{\alpha\beta}$. The tensor $n_\alpha n_\beta$ is a degenerate, one-dimensional tensor with eigen-direction parallel to $\hat{\boldsymbol{n}}$ and trace unity. In two dimensions $\hat{\boldsymbol{t}}$ defines the tangential direction modulo the sign. In both two and three dimensions, one can use $\hat{\boldsymbol{t}} := \delta\boldsymbol{l}^t/|\delta\boldsymbol{l}^t|$ as definition if $|\delta\boldsymbol{l}^t| > 0$. In three dimensions, this allows the definition of a third degenerate tensor perpendicular to both $\hat{\boldsymbol{n}}$ and $\hat{\boldsymbol{t}}$ via $s_\alpha s_\beta := 1_{\alpha\beta} - n_\alpha n_\beta - t_\alpha t_\beta$.

2.2 Change of potential energy density

The potential energy density,

$$u = \frac{1}{2V}\left(k\boldsymbol{\Delta}^2 + k^t\boldsymbol{\vartheta}^2\right) \ , \tag{4}$$

also changes due to a deformation, where k and k^t are the spring stiffness in normal and tangential direction, respectively (the prefactor of the quadratic term in the series expansion of the interaction potential), and the volume V will be specified later, since it depends on the configuration of the particles in the neighborhood.

Due to the displacement of one pair of particles, the change in potential energy density is

$$\begin{aligned} \delta u \ &= \ \delta u^n + \delta u^t \\ &\approx \ \frac{1}{V}\,\boldsymbol{f}^* \cdot \boldsymbol{\varepsilon} \cdot \boldsymbol{l} \ , \end{aligned} \tag{5}$$

with the actual force $\boldsymbol{f} = k\boldsymbol{\Delta} + k^t\boldsymbol{\vartheta}$, the force after displacement $\boldsymbol{f}' = \boldsymbol{f} + \delta\boldsymbol{f}$, and the mean $\boldsymbol{f}^* = (\boldsymbol{f} + \boldsymbol{f}')/2$. (The asterisk is dropped in the following for the sake of simplicity $\boldsymbol{f} \approx \boldsymbol{f}^*$). Note the nice symmetry of the problem with respect to an exchange of the present configuration (unprimed) and the deformed configuration (primed).

[1] Summation over equal indices is implied

2.3 The stress tensor

From the potential energy density, we obtain the transposed stress from the response to a virtual deformation by differentiation of u with respect to the deformation tensor components

$$\sigma_{\beta\alpha} \;=\; \frac{1}{V} f_\alpha l_\beta \ . \tag{6}$$

For the result in Eq. (6), in symbolic notation: $\boldsymbol{\sigma} = \boldsymbol{l}\boldsymbol{f}/V$, the partial derivative with respect to the deformation tensor was replaced by the identity tensors $1_{\alpha a}1_{\beta b}$ and the higher order terms in Eq. (5) were neglected.

The change in stress due to the virtual deformation $\boldsymbol{\varepsilon}$ is

$$\delta\boldsymbol{\sigma} = \boldsymbol{\sigma}' - \boldsymbol{\sigma} = \frac{1}{V}\boldsymbol{l}\left(k\delta\boldsymbol{l}^n + k^t\delta\boldsymbol{l}^t\right) = \frac{1}{V}\boldsymbol{l}\ \delta\boldsymbol{f} \ , \tag{7}$$

since the overlaps $\boldsymbol{\Delta}$ and $\boldsymbol{\vartheta}$ depend on the tensor $\boldsymbol{\epsilon}$, whereas $\boldsymbol{l}$ does not. The work due to a virtual stress change $\delta\boldsymbol{\sigma}^T\!:\boldsymbol{\epsilon} = \delta u$ thus allows to regard $\boldsymbol{\epsilon}$ as the conjugate tensor-variable to $\boldsymbol{\sigma}$.

Since $\boldsymbol{l}$ and $\boldsymbol{\Delta}$ are parallel to $\hat{\boldsymbol{n}}$ and $\boldsymbol{\vartheta}$ is parallel to $\hat{\boldsymbol{t}}$, we can rewrite the stress tensor

$$\sigma_{\alpha\beta} \;=\; \frac{kl\Delta}{V} n_\alpha n_\beta + \frac{k^t l\vartheta}{V} n_\alpha t_\beta \ , \tag{8}$$

with $\Delta = |\boldsymbol{\Delta}|$ and $\vartheta = |\boldsymbol{\vartheta}|$. Note that the dyadic product of the normal vectors $n_\alpha n_\beta$ is symmetric (and degenerate one-dimensional) by definition, whereas $n_\alpha t_\beta$ is not necessarily symmetric, traceless and two-dimensional.

2.4 The stiffness tensor

The partial derivative of the stress tensor with respect to the deformation leads to the stiffness tensor

$$C_{\alpha\beta\gamma\phi} = \;=\; \frac{l^2}{V}\left(k\, n_\alpha n_\beta n_\gamma n_\phi + k^t n_\alpha t_\beta n_\gamma t_\phi\right) \ , \tag{9}$$

where the change of the deformation in normal and tangential direction was used. The additional derivative which should occur in Eq. (9) leads to terms proportional to Δ/l which are neglected in the following, if the overlap is much smaller than the distance between the particle centers.

3 One particle with C neighbors

Given the tensor-elements based on single contacts, one possibility is to compute the tensor in average over all contacts of one particle. In a further step, the averages are performed over all contacts within an averaging volume V which is typically much larger than one particle and thus can contain many contacts. For the sake of simplicity, the simplest averaging approach is used here, i.e. a contact is taken into account if the corresponding particle-center lies within the averaging volume. This corresponds to a pre-averaging over single particles and then subsequent averaging over the particles in the volume. In an equation this reads

$$Q = \langle Q \rangle = \frac{1}{V}\sum_{p\in V} V^p Q^p \ , \tag{10}$$

where Q is the quantity to be averaged and $Q^p = \sum_{c=1}^{C} Q^c$ is the pre-averaged particle quantity with the contact quantity Q^c. Note that the criterion $p \in V$ in the sum has to be discussed [4], even though we will use the simplest approach in the following, i.e. particles with their center in the averaging volume are taken into account.

3.1 The Fabric Tensor

For one particle, the fabric tensor is

$$F^p_{\alpha\beta} = \sum_{c=1}^{C} n_\alpha n_\beta \ , \tag{11}$$

with the trace $\mathrm{tr}\boldsymbol{F}^p = F^p_{\gamma\gamma} = C$. For one unit-cell with volume V^u, the fabric tensor can be defined as

$$F^u_{\alpha\beta} = \frac{V^p}{V^u} \sum_{c=1}^{C} n_\alpha n_\beta \ . \tag{12}$$

so that $\mathrm{tr}\boldsymbol{F}^u = F^u_{\gamma\gamma} = \nu C$ is a contact number density with the volume fraction $\nu = V^p/V^u$. In a disordered system, the relation between fabric, density and contact number is more complicated [5] and an average over many particles

$$F_{\alpha\beta} = \frac{1}{V} \sum_{p \in V} V^p \sum_{c=1}^{C} n_\alpha n_\beta \tag{13}$$

is the method of choice. Note that we will drop the super-script u for unit-cell in the following since the equations are identical to those with arbitrary averaging volume when the sum over the particles reduces to one term.

3.2 The Stress Tensor

For C contact partners, one obtains the average stress in the particle

$$\sigma^p_{\alpha\beta} = \frac{1}{V^p} \sum_{c=1}^{C} l^c_\alpha f^c_\beta \ , \tag{14}$$

where the definition of the contact force $f^c_\alpha = k\Delta^c_\alpha + k^t \vartheta^c_\alpha$ at contact c was used.

In a larger volume V, one obtains the stress

$$\sigma_{\alpha\beta} = \frac{1}{V} \sum_{p \in V} \sum_{c=1}^{C} l^c_\alpha f^c_\beta \ , \tag{15}$$

where the particle volumes cancel due to the weighting condition in Eq. (10).

3.3 The stiffness tensor

The stiffness tensor for one homogeneous, spherical particle with equal branch vectors $l = l^c$ and spring constants $k = k^c$ and $k^t = (k^t)^c$ is

$$C^p_{\alpha\beta\gamma\phi} = \frac{l^2}{V^p} \left(k \sum_{c=1}^{C} n^c_\alpha n^c_\beta n^c_\gamma n^c_\phi + k^t \sum_{c=1}^{C} n^c_\alpha t^c_\beta n^c_\gamma t^c_\phi \right) \ , \tag{16}$$

and the generalization to an arbitrary volume is evident.

4 Simulation Results

4.1 Model System

One possibility to obtain information about the material behavior is to perform elementary tests in the laboratory. An alternative are simulations with the discrete element model (DEM) [1, 2, 6–11] and the average over the "microscopic" quantities in some averaging volume. The experiment chosen is the bi-axial box set-up, see Fig. 1, where the left and bottom walls are fixed, and stress- or strain-controlled deformation is applied. In the first case a wall is subject to a predefined pressure, in the second case, the wall is subject to a defined strain ε_{zz}. In a typical 'experiment', the top wall is strain controlled and slowly shifted downwards while the right wall moves stress controlled, dependent on the forces exerted on it by the material in the box. The strain-controlled position of the top wall as function of time t is here

$$z(t) = z_f + \frac{z_0 - z_f}{2}(1 + \cos \omega t) \ , \quad \text{with} \quad \varepsilon_{zz} = 1 - \frac{z}{z_0} \ , \tag{17}$$

where the initial and the final positions z_0 and z_f can be specified together with the rate of deformation $\omega = 2\pi f$ so that after a half-period $T/2 = 1/(2f)$ the extremal deformation is reached. With other words, the cosine is active for $0 \le \omega t \le \pi$. For larger times, the top-wall is fixed and the system can relax. The cosine function is chosen in order to allow for a smooth start-up and finish of the motion so that shocks and inertia effects are reduced, however, the shape of the function is arbitrary as long as it is smooth.

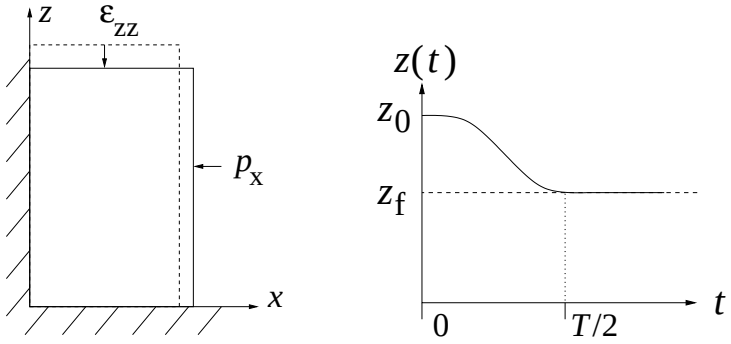

Figure 1: (Left) Schematic drawing of the model system. (Right) Position of the top-wall as function of time for the strain-controlled situation.

The stress-controlled motion of the side-wall is described by

$$m_w \ddot{x}(t) = F(t) - pz(t) - \gamma_w \dot{x}(t) \ , \tag{18}$$

where m_w is the mass of the right side wall. Large values of m_w lead to slow adaption, small values allow for a rapid adaption to the actual situation. Three forces are active: (i) the force $F_x(t)$ due to the bulk material, (ii) the force $-p_x z(t)$ due to the external pressure, and (iii) a strong frictional force which damps the motion of the wall so that oscillations are reduced.

4.2 Discrete Particle Model

The elementary units of granular materials are mesoscopic grains which deform under stress. Since the realistic modeling of the deformations of the particles is much too complicated,

we relate the interaction force to the overlap δ of two particles, see Fig. 2. Note that the evaluation of the inter-particle forces based on the overlap may not be sufficient to account for the inhomogeneous stress distribution inside the particles. Consequently, our results presented below are of the same quality as the simple assumptions about the force-overlap relation.

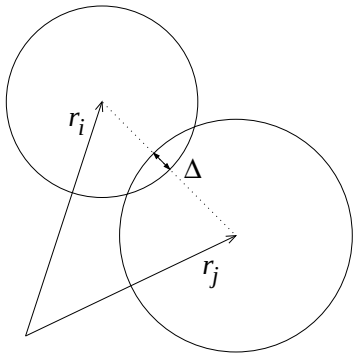

Figure 2: (Left) Two particle contact with overlap Δ.

If all forces $\boldsymbol{f}_i$ acting on the particle i, either from other particles, from boundaries or from external forces, are known, the problem is reduced to the integration of Newton's equations of motion for the translational and rotational degrees of freedom

$$m_i \frac{\mathrm{d}^2}{\mathrm{d}t^2}\boldsymbol{r}_i = \boldsymbol{f}_i \ , \quad \text{and} \quad I_i \frac{\mathrm{d}^2}{\mathrm{d}t^2}\boldsymbol{\varphi}_i = \boldsymbol{t}_i \tag{19}$$

with the mass m_i of particle i, its position $\boldsymbol{r}_i$ the total force $\boldsymbol{f}_i = \sum_c \boldsymbol{f}_i^c$ acting on it due to contacts with other particles or with the walls, its moment of inertia I_i, its angular velocity $\boldsymbol{\omega}_i = \mathrm{d}\boldsymbol{\phi}_i/\mathrm{d}t$ and the total torque $\boldsymbol{t}_i = \sum_c \boldsymbol{l}_i^c \times \boldsymbol{f}_i^c$.

4.2.1 Normal Contact Model

Two particles i and j interact only if they are in contact so that their overlap

$$\Delta = (\boldsymbol{r}_i - \boldsymbol{r}_j) \cdot \boldsymbol{n} - (1/2)(d_i + d_j) \tag{20}$$

is negative, $\Delta < 0$, with the unit vector $\boldsymbol{n} = \boldsymbol{n}_{ij} = (\boldsymbol{r}_i - \boldsymbol{r}_j)/|\boldsymbol{r}_i - \boldsymbol{r}_j|$ pointing from j to i. The force on particle i, from particle j can be decomposed into normal and tangential part as $\boldsymbol{f}_{ij} = f_{ij}^n \boldsymbol{n} + f_{ij}^t \boldsymbol{t}$. The simplest normal force is a linear spring and a linear dashpot

$$f_{ij}^{\mathrm{diss}} = k\Delta + \gamma_0 \dot{\delta} \tag{21}$$

with spring constant k and some damping coefficient γ_0. The half-period of a vibration around the equilibrium position can be computed, and one obtains a typical response time on the contact level,

$$t_c = \frac{\pi}{\omega} \ , \quad \text{with} \quad \omega = \sqrt{\frac{k}{m_{12}} - \eta_0^2} \ , \tag{22}$$

the eigenfrequency of the contact, and the rescaled damping coefficient $\eta_0 = \gamma_0/(2m_{12})$.

4.2.2 Tangential Contact Model

The force in tangential direction is implemented in the spirit of Cundall and Strack [6] who introduced a tangential spring in order to account for static friction. Various authors have used this idea and numerous variants were implemented, see [12] for a summary and discussion.

Since we use a formulation which is generalized to dimensions $\mathcal{D} = 2$ and $\mathcal{D} = 3$, it is necessary to repeat the model and define the implementation. The tangential force is coupled to the normal force via Coulombs law, i.e. $f_t \leq \mu^s f_n$, where for the limit case one has dynamic friction with $f_t = \mu^d f_n$. The dynamic and the static friction coefficients follow, in general, the relation $\mu^d \leq \mu^s$. However, for the following simulations we will apply $\mu = \mu^d = \mu^s$. The static situation requires an elastic spring in order to allow for a restoring force, i.e. a non-zero remaining tangential force in static equilibrium due to activated Coulomb friction.

If $f_n > 0$, the tangential force is active, and we project the tangential spring into the actual tangential plane [2]

$$\boldsymbol{\xi} = \boldsymbol{\xi}' - \boldsymbol{n}(\boldsymbol{n} \cdot \boldsymbol{\xi}') \ , \tag{23}$$

where $\boldsymbol{\xi}'$ is the old spring from the last iteration. This action is relevant only for an already existing spring, if the spring is new, the tangential spring-length is zero anyway, however, its change is well defined. The tangential velocity is

$$\boldsymbol{v}_t = \boldsymbol{v}_{ij} - \boldsymbol{n}(\boldsymbol{n} \cdot \boldsymbol{v}_{ij}) \ , \tag{24}$$

with the total relative velocity

$$\boldsymbol{v}_{ij} = \boldsymbol{v}_i - \boldsymbol{v}_j + a_i \boldsymbol{n} \times \boldsymbol{\omega}_i + a_j \boldsymbol{n} \times \boldsymbol{\omega}_j \ . \tag{25}$$

Next, we calculate the tangential test-force as the sum of the tangential spring and a tangential viscous force (in analogy to the normal viscous force)

$$\boldsymbol{f}_t^0 = -k_t \boldsymbol{\xi} - \gamma_t \boldsymbol{v}_t \ , \tag{26}$$

with the tangential spring stiffness k_t and the tangential dissipation parameter γ_t. As long as $|\boldsymbol{f}_t^0| \leq f_C^s$, with $f_C^s = \mu^s f_n$, one has static friction and, on the other hand, if the limit $|\boldsymbol{f}_t^0| > f_C^s$ is reached, sliding friction is active with $f_C^d = \mu^d f_n$. (As soon as $|\boldsymbol{f}_t^0|$ becomes smaller than f_C^d, static friction is active again.) In the former, static case, the tangential spring is incremented

$$\boldsymbol{\xi}' = \boldsymbol{\xi} + \boldsymbol{v}_t \Delta t_{\mathrm{MD}} \ , \tag{27}$$

to be used in the next iteration in Eq. (23), and the force $\boldsymbol{f}_t = \boldsymbol{f}_t^0$ from Eq. (26) is used. In the latter, sliding case, the tangential spring is adjusted to a length which is consistent with Coulombs condition

$$\boldsymbol{\xi}' = -\frac{1}{k_t} f_C^d \boldsymbol{t} \ , \tag{28}$$

with the tangential unit vector, $\boldsymbol{t} = \boldsymbol{f}_t^0 / |\boldsymbol{f}_t^0|$, defined by Eq. (26), and thus the magnitude of the Coulomb force is used. Inserting $\boldsymbol{\xi}'$ into Eq. (26) leads to $\boldsymbol{f}_t^0 \approx -f_C \boldsymbol{t} - \gamma_t \boldsymbol{v}_t$. Note that $\boldsymbol{f}_t^0$ and $\boldsymbol{v}_t$ are not necessarily parallel in three dimensions. However, the mapping in Eq. (28) works always, rotating the new spring such that the direction of the frictional force is

[2] This is necessary, since the frame of reference of the contact may have rotated since the last time-step

unchanged and, at the same time, limiting the spring in length according to Coulombs law. In short notation this reads

$$\boldsymbol{f}_t = +\min\left(f_C, |\boldsymbol{f}_t^0|\right)\boldsymbol{t} \ , \tag{29}$$

where f_C follows the selection rules described above.

Note that the tangential force described above is identical to the classical Cundall-Strack spring only in the limits $\mu = \mu^s$ and $\gamma_t = 0$. The sequence of computations and the definitions and mappings into the tangential direction, however, is new to our knowledge in so far that it can be easily generalized in three dimensions as well as in two.

4.2.3 Background Friction

Note that the viscous dissipation takes place in a two-particle contact. In the bulk material, where many particles are in contact with each other, dissipation is very inefficient due to long-wavelength cooperative modes of motion [13, 14]. Therefore, an additional damping with the background is introduced, so that the total force on particle i is

$$\boldsymbol{f}_i = \sum_j (f_{ij}^{\mathrm{hys}} + f_{ij}^{\mathrm{diss}})\boldsymbol{n} + \boldsymbol{f}_t - \gamma_{\mathrm{b}}\boldsymbol{v}_i \ , \tag{30}$$

with the damping artificially enhanced in the spirit of a rapid equilibration.

4.3 Simulation Results

The systems examined in the following contain $N = 1950$ particles with radii a_i randomly drawn from a homogeneous distribution with minimum $a_{\min} = 0.5\,10^{-3}\,\mathrm{m}$ and maximum $a_{\max} = 1.5\,10^{-3}\,\mathrm{m}$. The masses $m_i = (4/3)\rho\pi a_i^3$, with the density $\rho = 2\,10^3 \mathrm{kg\,m^{-3}}$, are computed as if the particles were spheres. This is an artificial choice and introduces some dispersity in mass in addition to the dispersity in size. However, since we are mainly concerned about slow deformation and equilibrium situations, the choice for the calculation of mass should not matter. The total mass of the particles in the system is thus $M \approx 0.02\,\mathrm{kg}$ with the typical reduced mass of a pair of particles with mean radius, $m_{12} \approx 0.42\,10^{-5}\,\mathrm{kg}$. If not explicitly mentioned, the material parameters are $k = 10^5\,\mathrm{N\,m^{-1}}$, and $\gamma_0 = 0.1\,\mathrm{kg\,s^{-1}}$.

4.3.1 Initial Configuration

Initially, the particles are randomly distributed in a huge box, with rather low overall density. Then the box is compressed, either by moving the walls to their desired position, or by defining an external pressure $p = p_{\mathrm{x}} = p_{\mathrm{z}}$, in order to achieve an isotropic initial condition. Starting from a relaxed, isotropic initial configuration, the strain is applied to the top wall and the response of the system is examined. In Fig. 3, snapshots from a typical simulation are shown during compression.

4.4 Averaged Quantities

In the following, simulations are presented for the side pressure $p = 20$ only. A more detailed study involving various $p = 20$, 40, 100, 200, 400, and 500 is in preparation [15]. There, the behavior of all the averaged scalar and tensor variables during the simulations is examined in

$\epsilon_{zz} = 0$ $\epsilon_{zz} = 0.011$ $\epsilon_{zz} = 0.091$ $\epsilon_{zz} = 0.120$

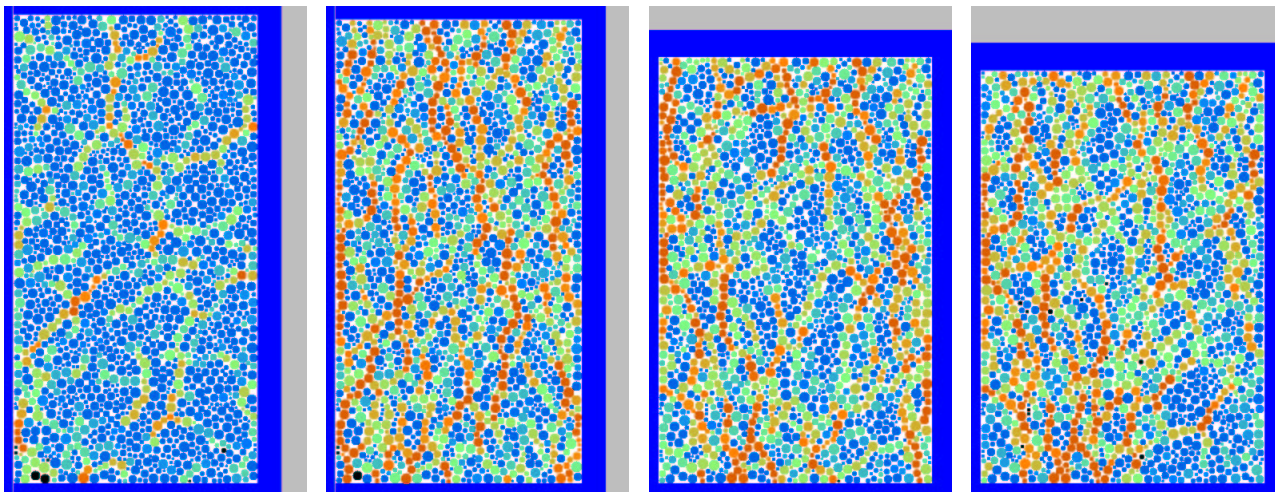

Figure 3: Snapshots of the simulation at different ϵ_{zz} for side pressure $p = 200$. The color code corresponds to the potential energy of each particle, decaying from red, green (bright) to blue and black (dark).

detail for situations with low and high confining pressure. Here we focus in the fabric and the stiffness tensor only.

The averages are performed such that ten per-cent of the total volume are disregarded in the vicinity of each wall in order to avoid boundary effects. A particle contact is taken into account for the average if the contact point lies within the averaging volume V.

4.4.1 Fabric Tensor

The fabric tensor

$$F_{\alpha\beta} = \frac{1}{V} \sum_{c \in V} (V^p + V^q) n_\alpha n_\beta \ . \tag{31}$$

is computed as a sum over all contacts in the averaging volume with the volume of the particles p and q which share the contact c.

The trace of the fabric first rapidly increases, due to the initial compression, then decays, due to the dilation, and eventually reaches an almost stationary value. This stationary contact number density is slightly larger for higher pressure, whereas there is no evident difference for the deviator and the orientation. The former grows to values around 0.5 and the latter remains close to zero, i.e. the fabric is well anisotropic, but not tilted away from the box geometry.

4.4.2 Stiffness tensor

The normal contributions $\boldsymbol{C}^n$ are plotted in Fig. 5, in units of k. The elements with an even number of one/two-indices are non-zero, whereas the entries with an odd number are always much smaller (open symbols). The difference between C^n_{1111} and C^n_{2222} indicates the anisotropy that is build up during the experiment, i.e. the material becomes stronger in vertical than in horizontal direction. The small values of C^n_{1112} and C^n_{1222} (small dots) indicate that the eigen-system is not tilted much from the cartesian and, expressed in terms material behavior, mean

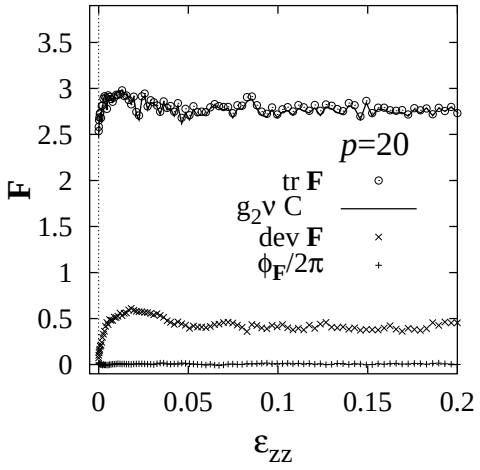

Figure 4: Fabric tensor, contact number density, deviator fabric, and fabric orientation ϕ_F. The contact number density is corrected by a factor $g_2 \approx 1.088$ which accounts for the polydisperse size-distribution [5]

that the material does neither respond with a shear stress to a linear deformation nor with a linear stress to a simple shear deformation.

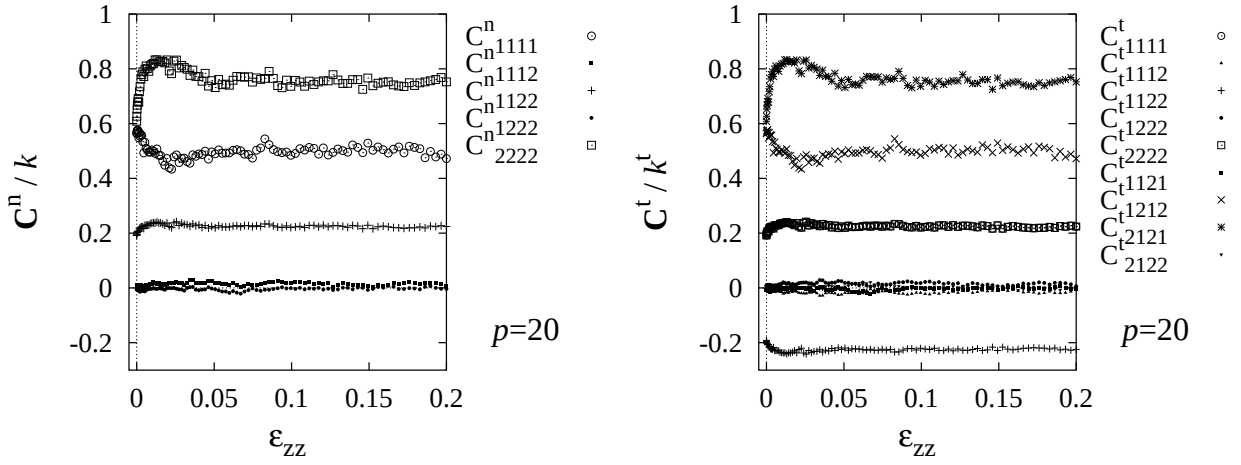

Figure 5: (Left) Normal contributions to the tensor $\boldsymbol{C}$. (Right) Tangential contributions.

The tangential contributions $\boldsymbol{C}^t$ are plotted in Fig. 5, in units of k^t, where $\alpha = k^t/k^n$ is the ratio of tangential and normal stiffness. Here, the result is more complicated due to more different entries: The entries $C^t_{1111} = C^t_{2222} = \alpha C^n_{1122}$ (open symbols) are now identical and behave like the entry C^n_{1122}. In contrast, the entry $C^t_{1122} = -\alpha C^n_{1122}$ (plus symbol) has negative sign and cancels the normal entry if summed up with $\alpha = 1$. The entries C^t_{1112} and C^t_{1222} (small dots) are again very small, and so are the new, different entries C^t_{1121} and C^t_{2122} (small dots), like in the normal tensor. The remaining two entries behave like the major entries in the normal tensor, i.e. $C^t_{1212} = \alpha C^n_{1111}$ and $C^t_{2121} = \alpha C^n_{2222}$ (x-symbol and star-symbol).

As could be expected from the experimental setup, the stiffness matrix behaves such that the material builds up strength against the direction of compression, and becomes weaker in the perpendicular direction. The tangential springs add up in stiffness to the normal springs according to their microscopic spring stiffness. Only the entry C_{1122} is significantly negative

and may reduce the total stiffness. The behavior of the normal stiffness tensor is reflected in the tangential stiffness tensor entries, however, in different ones. Finally, we note that the magnitude of the stiffness tensor entries is higher for larger external pressure.

When the tiny entries of $\boldsymbol{C}$ are examined closer, one observes that $\alpha C^n_{1112} = C^t_{1222}$ and $\alpha C^n_{1222} = C^t_{1121}$, while the entries $C^t_{1112} = -C^t_{1222}$ and $C^t_{2122} = -C^t_{1121}$ have the corresponding opposite sign. However, as mentioned above, the magnitude of these entries is very small as compared to those entries with an even number of one/two-indices.

As a last interesting observation, we remark that the entry C^n_{1112} is larger in magnitude than C^n_{1222}. We relate this to the fact that the left and bottom wall of the simulation volume are fixed which breaks the symmetry of the problem and creates a preferred direction of tilt induced by the shear deformation.

5 Summary

As brief summary, we conclude that there are three entries for the stiffness tensor, scaled by the microscopic spring stiffness used for the simulation. The normal contacts contribute the shear modulus and two (different) normal moduli. The reason for this small number of quantities is the biaxial geometry that fixes the eigen-system of the tensorial quantities. The stiffness tensor due to the tangential springs also scales with the corresponding spring stiffness and has also only three independent magnitudes (one entry of them being negative).

In the biaxial geometry we observe clear anisotropy of the fabric and the stiffness tensor. The magnitude of anisotropy is maximal at the point of maximum stiffness. Then, due to shear band localization, the material becomes softer and less anisotropic, until the measured quantities saturate in the critical flow regime.

The microscopic and structural reasons for the limit in anisotropy is unclear as well as the detailed relation between stress, strain, and anisotropy. Future research involves a more detailed parameter study and three dimensional simulations of similar systems.

Acknowledgements

We thank J. Tomas, E. Clément, N. P. Kruyt, and C. Thornton for helpful discussions and acknowledge the support of the Deutsche Forschungsgemeinschaft (DFG).

References

[1] H. J. Herrmann, J.-P. Hovi, and S. Luding, editors. *Physics of dry granular media - NATO ASI Series E 350*, Dordrecht, 1998. Kluwer Academic Publishers.

[2] P. A. Vermeer, S. Diebels, W. Ehlers, H. J. Herrmann, S. Luding, and E. Ramm, editors. *Continuous and Discontinuous Modelling of Cohesive Frictional Materials*, Berlin, 2001. Springer. Lecture Notes in Physics 568.

[3] Y. Kishino, editor. *Powders & Grains 2001*, Rotterdam, 2001. Balkema.

[4] M. Lätzel, S. Luding, and H. J. Herrmann. Macroscopic material properties from quasi-static, microscopic simulations of a two-dimensional shear-cell. *Granular Matter*, 2(3):123–135, 2000. cond-mat/0003180.

[5] M. Madadi, O. Tsoungui, M. Lätzel, and S. Luding. On the fabric tensor of static, polydisperse granular materials. in preparation, 2001.

[6] P. A. Cundall and O. D. L. Strack. A discrete numerical model for granular assemblies. *Géotechnique*, 29(1):47–65, 1979.

[7] Y. M. Bashir and J. D. Goddard. A novel simulation method for the quasi-static mechanics of granular assemblages. *J. Rheol.*, 35(5):849–885, 1991.

[8] S. van Baars. *Discrete Element Analysis of Granular Materials.* PhD thesis, Technische Universiteit Delft, Delft, Nederlands, 1996.

[9] C. Thornton. Numerical simulations of deviatoric shear deformation of granular media. *Géotechnique*, 50(1):43–53, 2000.

[10] C. Thornton and S. J. Antony. Quasi-static deformation of a soft particle system. *Powder Technology*, 109(1-3):179–191, 2000.

[11] N. P. Kruyt and L. Rothenburg. Statics of the elastic behavior of granular materials. *Int. J. of Solids and Structures*, 38:4879–4899, 2001.

[12] L. Brendel and S. Dippel. Lasting contacts in molecular dynamics simulations. In H. J. Herrmann, J.-P. Hovi, and S. Luding, editors, *Physics of Dry Granular Media*, page 313, Dordrecht, 1998. Kluwer Academic Publishers.

[13] S. Luding, E. Clément, A. Blumen, J. Rajchenbach, and J. Duran. The onset of convection in molecular dynamics simulations of grains. *Phys. Rev. E*, 50:R1762, 1994.

[14] S. Luding, E. Clément, A. Blumen, J. Rajchenbach, and J. Duran. Anomalous energy dissipation in molecular dynamics simulations of grains: The "detachment effect". *Phys. Rev. E*, 50:4113, 1994.

[15] S. Luding. Micro-macro transition for anisotropic, periodic, elastic solids. in preparation, 2003.